

RSC Advances



This is an *Accepted Manuscript*, which has been through the Royal Society of Chemistry peer review process and has been accepted for publication.

Accepted Manuscripts are published online shortly after acceptance, before technical editing, formatting and proof reading. Using this free service, authors can make their results available to the community, in citable form, before we publish the edited article. This *Accepted Manuscript* will be replaced by the edited, formatted and paginated article as soon as this is available.

You can find more information about *Accepted Manuscripts* in the [Information for Authors](#).

Please note that technical editing may introduce minor changes to the text and/or graphics, which may alter content. The journal's standard [Terms & Conditions](#) and the [Ethical guidelines](#) still apply. In no event shall the Royal Society of Chemistry be held responsible for any errors or omissions in this *Accepted Manuscript* or any consequences arising from the use of any information it contains.

Synthesis of Magnetic Graphene Oxide-Containing Nanocomposite Hydrogels for Adsorption of Crystal Violet from Aqueous Solution

Ali Pourjavadi*, Mojtaba Nazari, Seyed Hassan Hosseini

Polymer Research Laboratory, Department of Chemistry, Sharif University of Technology, Tehran, Iran

E-mail address: purjavadi@sharif.edu; Phone/fax: (982)166165311

Abstract

Magnetic nanocomposite hydrogels containing different amounts of graphene oxide were synthesized and characterized by FTIR, XRD, TGA, SEM, TEM, VSM and UV-vis spectroscopy. The prepared hydrogels were used as adsorbents for removal of a cationic dye, crystal violet, from water. Kinetic and isotherm of adsorption and the effect of different experimental conditions such as graphene oxide content, pH of the solution, contact time, adsorbent dosage and initial dye concentration on adsorption capacity were then investigated. Parameters related to kinetic and isotherm models were calculated and discussed. It was found that adsorption is well-described by pseudo-second-order kinetic and Langmuir isotherm models, respectively. The synthesized adsorbents showed high efficiency in removal of crystal violet and a very high adsorption capacity was obtained (769.23 mg g^{-1}). No significant loss of removal efficiency was observed even after five cycles of adsorption.

Keywords: Dye adsorption, graphene oxide, nanocomposite hydrogels, crystal violet, magnetic nanoparticles

Introduction

Dyes are organic colorant compounds that are extensively used in many different industrial fields such as textile, tanning, paper, food and cosmetics.^{1, 2} Discharge of dyes into the environment can contaminate underground water and cause serious health and biological problems. Crystal violet (CV) is a common cationic dye which belongs to triphenylmethane group. This dye is widely used as colorant, biological stain and veterinary medicine. CV has been found to have harmful effects on human and has been suspected to cause cancer.³ Therefore, it is very important to separate and remove dyes from wastewater. There are many different methods for removal of dyes from water such as adsorption,⁴ photodegradation,⁵ coagulation,⁶ ion exchange⁷ and membrane filtration.⁸ However, adsorption is the most attractive method because of its high efficiency, ease of operation and cost effectiveness. A wide range of different organic and inorganic adsorbents such as activated carbon,⁹ clays,¹⁰ carbon nanotubes,¹¹ and polymeric materials^{12, 13} have been prepared and used for dye adsorption. However, in many cases, the prepared adsorbents have low surface area, low adsorption capacity and weak mechanical strength in severe conditions. Therefore, it is still necessary to develop mechanically strong adsorbents with high efficiency.

Polymeric hydrogels are very attractive for dye adsorption since water can easily diffuse through the hydrophilic polymer network and dissolved dyes can interact strongly with numerous functional groups present in the structure of polymer chains. The adsorption of dyes strongly depends on the structure and composition of the hydrogels. Polymeric hydrogels with different compositions have been used for adsorption of cationic and anionic dyes.¹⁴⁻¹⁶ Hydrogels with negative charges in their structures are effective in removal of cationic dyes, while positively charged hydrogels are appropriate for removal of anionic dyes.¹⁴ Zwitterionic hydrogels can be used for both cationic and anionic dyes.¹² However, weak mechanical strength of the hydrogels is one of their drawbacks that limits the

application of hydrogels especially for repeated cycles of adsorption. In many cases hydrogels are filled with inorganic materials to improve their mechanical properties. Clays¹⁷ and carbonaceous materials such as carbon nanotube,¹⁸ and graphene¹⁹ have been used for this purpose. It was also found that the presence of inorganic materials increases adsorption capacity of dyes.²⁰

Graphene oxide (GO) is a carbonaceous material that have attracted much attention in recent years.^{21, 22} GO is produced by oxidation of graphite which leads to introducing different oxygen-containing functional groups such as hydroxyl, epoxy and carbonyl groups. These functional groups can interact with dye molecules through hydrogen bonds and electrostatic interactions. These properties make GO a good candidate for dye adsorption.

Incorporating of GO into hydrogels leads to the formation of nanocomposite adsorbents with high mechanical strength.²³ The presence of GO not only improves physical properties of hydrogel but also increases its adsorption capacity. Although it has been shown that GO itself and also polymeric hydrogels can be used as dye adsorbents,²⁴⁻²⁶ synthesis of GO-based nanocomposites can combine properties of both GO and hydrogels. As a result, adsorbents with high mechanical strength and adsorption capacity could be obtained. Although GO and its polymeric nanocomposites have being studied extensively in recent years, there are few reports in the field of GO-hydrogel nanocomposites for dye adsorption.

Considering the advantages of GO and magnetic nanoparticles, in this paper we are going to prepare hydrogel nanocomposites containing these two inorganic materials. Since there are many polar functional groups on the surface of GO and because of its high specific surface area, it is expected that the presence of GO increases adsorption capacity of the hydrogel. It also can act as reinforcement filler which increases mechanical strength of hydrogels, as reported by Fan *et al.*²³ The presence of magnetic nanoparticles in the structure of hydrogels

facilitates separations of the hydrogels so that they can be separated easily after adsorption process by using a magnet.^{27,28}

Herein, we report synthesis and characterization of a novel magnetic nanocomposite hydrogel containing GO. The nanocomposite has consisted of hydrogel in which GO sheets and magnetic iron oxide nanoparticles are entrapped. The polymeric network of hydrogel is composed of a natural polymer, starch, and a hydrophilic polymer, poly(2-acrylamido-2-methylpropane sulfonic acid) (PAMPS). The synthesized nanocomposite was used as a dye adsorbent and its ability for removal of CV was studied. The effect of different experimental conditions on dye adsorption was also investigated.

Materials and methods

Materials

Graphite powders were obtained from Aldrich. 2-Acrylamido-2-methylpropane sulfonic acid (AMPS), ammonium persulfate (APS), N,N'-methylenebisacrylamide (MBA), tetraethylorthosilicate (TEOS) and starch were purchased from Merck and used without further purification.

Fourier transform infrared (FTIR) spectra were collected on an ABB Bomem MB 100 spectrophotometer. Scanning electron microscopy (SEM) images were taken on Philips, XL30 instrument. Transmission electron microscopy (TEM) images were taken using a Philips CM30 electron microscope. X-ray diffraction (XRD) patterns were recorded on a Siemens D5000 (Germany) diffractometer with monochromatized Cu K_α radiation. Thermogravimetric analysis (TGA) was conducted using a Perkin Elmer Pyris1 instrument from 30 to 600 °C with heating rate of 10 °C/min under nitrogen atmosphere. Magnetization measurements were performed by a model 7400 vibrating sample magnetometer (VSM). UV-vis spectroscopy was performed using a Perkin Elmer lambda 25 spectrophotometer.

Synthesis of GO

GO was synthesized by oxidation of natural graphite powder according to an improved Hummers method.²⁹ In a typical run, 1 g graphite was weighed in a round bottom flask and 120 mL H₂SO₄ and 13 mL H₃PO₄ were added to it. The flask was put in an oil bath and 6 g KMnO₄ was gradually added at 50 °C. After 12 hours stirring, the flask was cooled to 0 °C and 200 mL water and 3 mL H₂O₂ were added to the flask. The resulting product was washed three times with HCl solution (5% wt) and five times with water and then dried at 50 °C.

Synthesis of silica coated magnetic nanoparticles (MNP@SiO₂)

At first, Fe₃O₄ magnetic nanoparticles (MNPs) were synthesized by co-precipitation of FeCl₂·4H₂O and FeCl₃·6H₂O at pH=10. The resulting black particles were then coated with silica. 2 g of the synthesized MNPs were dispersed in 250 mL ethanol/water (4:1) solution in a round bottom flask. 15 mL TEOS was added and the pH of the solution was adjusted to 10 by using ammonia solution. The mixture was refluxed at 70 °C for 12 h. After cooling to room temperature, the product was washed several times with water and dried at 50 °C.

Synthesis of GO-Hydrogel nanocomposites

0.25 g MNP@SiO₂ and a known amount of GO were dispersed in 10 mL water by sonication for 30 minutes. Then, 0.25 g starch, 2.5 g AMPS (neutralized with NaOH) and 0.05 g MBA were added and the flask was placed in an oil bath. APS (0.05 g) was added to the flask and polymerization was performed at 70 °C and a hydrogel was obtained after 1h. After cooling to room temperature, the product was deswelled in acetone, dried at 50 °C and was ground and sieved through an 80-mesh sieve for further use.

Dye adsorption

Dye adsorption experiments were performed by a batch process at room temperature. Dye solutions (20 mg L⁻¹) were prepared by dissolving CV in water. The pH values of the

solutions were not adjusted except for investigating the effect of pH on dye adsorption. 10 mg of the powdered composites was added to 40 mL dye solution and the mixture was stirred at 500 rpm. A small amount of solution was taken in defined time intervals and the concentration of dye was determined by UV-vis spectroscopy using standard calibration curve. Measurements were conducted at λ_{\max} of CV (590 nm). All dye adsorption experiments were performed as mentioned here, unless otherwise noted. Adsorption capacity (q_e) and removal efficiency (R) are obtained as the following equations:

$$q_e = \frac{(C_0 - C_e)V}{m} \quad (1)$$

$$R = \frac{C_0 - C_e}{C_0} \times 100 \quad (2)$$

Where q_e is adsorption capacity (mg g^{-1}), C_0 and C_e are initial and equilibrium concentration of dye (mg L^{-1}), respectively, V is volume of the solution (L), and m is the mass of the adsorbent (g). C_0 and C_e are initial and equilibrium dye concentrations (mg g^{-1}), respectively.

Results and discussion

Synthesis of adsorbent

The hydrogel was prepared by graft copolymerization of AMPS onto the starch in the presence of MBA as crosslinker. MNPs were also used to induce magnetic properties in the hydrogels and to facilitate separation of adsorbent after adsorption process. MNPs were already coated with a layer of silica to enhance their stability in severe conditions and to prevent agglomeration of MNPs. As an anionic monomer, AMPS is able to interact with positively charged molecules through electrostatic interactions. Using starch introduces more hydroxyl groups in the structure of hydrogels and increases interaction with dyes. Moreover, the presence of starch as a natural polymer makes hydrogels more biodegradable and eco-friendly. In order to investigate the effect of GO on dye adsorption of the hydrogels,

nanocomposites with different amounts of GO were prepared. The amounts of GO used for preparation of hydrogel/GO nanocomposites (HGO) are listed in table 1.

Table 1 GO content of hydrogel/GO nanocomposites (HGO)

sample name	GO	
	g	%
HGO0	0	0
HGO1	0.03	1
HGO3	0.09	3
HGO5	0.15	5
HGO7	0.21	7

Polymerization was performed in the presence of GO and a hydrogel was formed while GO sheets were entrapped into the polymer network, as illustrated in Fig. 1. Since there are many polar functional groups in the structure of GO and also because of its sheet-like structure, it is expected that GO promote dye adsorption.

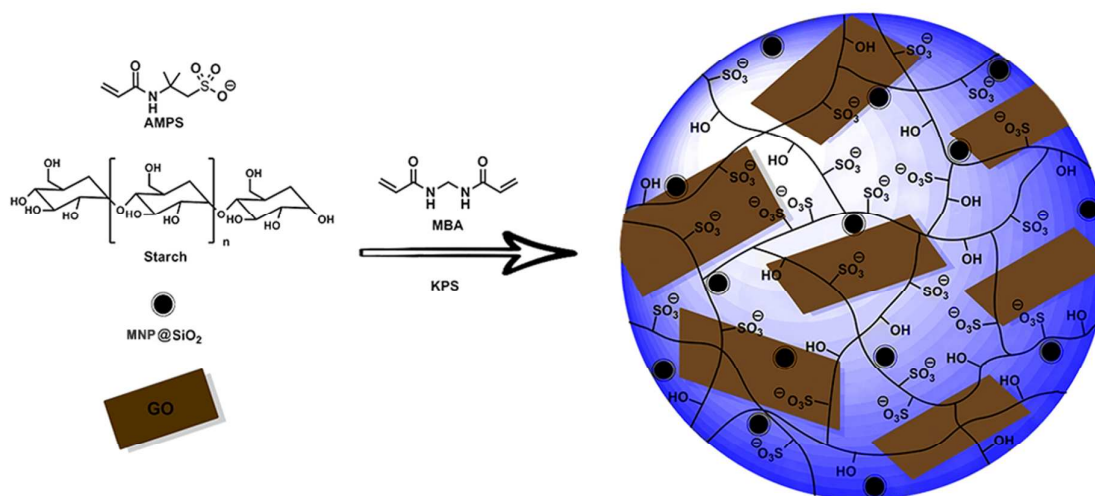


Fig. 1 Preparation of magnetic GO/hydrogel nanocomposite

The prepared hydrogels contain about 8 wt% starch in their structure. As a natural polysaccharide possessing D-glucose units, the presence of starch makes the prepared hydrogels more biodegradable. There are many reports in the literature in which starch was used in combination with synthetic monomers to produce biodegradable hydrogels.³⁰ Moreover, GO has also been recognized as a safe and non toxic material. Considering all these parameters the prepared hydrogels can be considered as an environmentally friendly adsorbent.

Characterization

XRD patterns of graphite, GO, MNPs and HGO1 are shown in Fig. 2. Graphite shows a very sharp diffraction peak at 2 theta value of 26° which is indexed to (002) plane with interlayer d-spacing of 3.4 Å. The XRD peak shifts downward to 2 theta value of 12° , after oxidation to GO (Fig. 2-b) and interlayer d-spacing increases to 8 Å due to the entering different functional groups and intercalation of water molecules between GO layers. XRD pattern of MNPs (Fig. 2-c) shows six peaks appeared at 2 theta values about 30, 36, 43, 53 57 and 62° corresponding to (220), (311), (400), (422), (511) and (440) planes, respectively. The six characteristic peaks of Fe_3O_4 are also present in the XRD pattern of HGO1 (Fig. 2-d). The broad peak appeared in 2θ range of 20 to 30° is related to amorphous silica layer. The absence of characteristic peak of GO at 2 theta value of 12° implies that GO was completely intercalated by polymeric chains and its crystalline structure was destroyed.

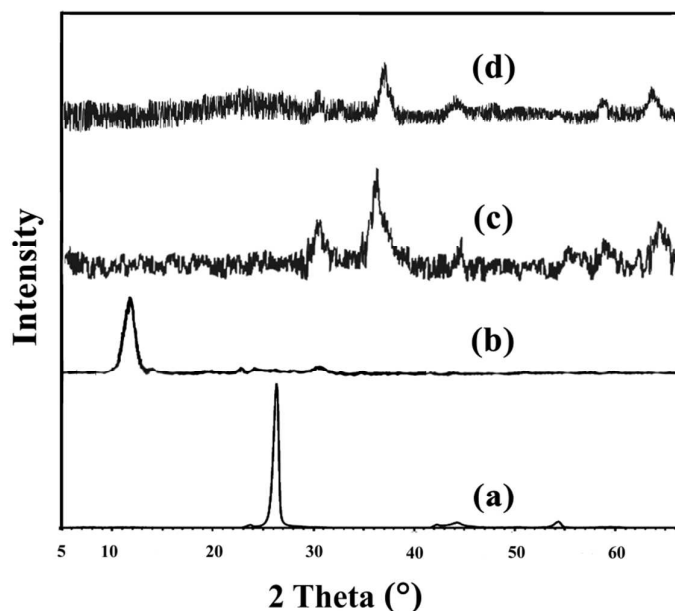


Fig. 2 XRD pattern of graphite (a), GO (b), MNPs (c) and HGO1 (d)

UV-vis spectrum of GO (Fig. S1-a of ESI) shows a peak at 229 nm which is related to $\pi \rightarrow \pi^*$ transitions of aromatic rings, and also a shoulder at 237 nm which is related to $n \rightarrow \pi^*$ transitions of carbonyl groups. The results indicate that graphite was successfully oxidized to GO. Elemental composition of GO was determined by CHN analysis and it was obtained that C, H and O content of GO is about 42, 3 and 55%, respectively. SEM (Fig. S1-b of ESI) and TEM (Fig. S1-c of ESI) images of GO shows that GO is composed of thin, large and wrinkled sheets with folded structure.

TEM image of MNP@SiO₂ is also shown in Fig. S1-d of ESI. Nanoparticles with average size about 10 nm and a narrow size distribution are observed. The grey shells are related to the silica layer coated on MNPs.

FTIR spectra of GO, MNPs, MNP@SiO₂ and GO-hydrogel nanocomposite are shown in Fig. 3. Peaks appeared at 3400, 1700, 1250 and 1050 cm⁻¹ in the spectrum of GO (Fig. 3-a) are related to O-H, C=O, C-O-C and C-O stretching vibrations, respectively. FTIR spectrum of MNPs (Fig. 3-b) shows a strong peak at 670 cm⁻¹ which is related to Fe-O stretching

vibration. After reaction with TEOS, a new intensive peak is appeared at 1100 cm^{-1} , attributing to Si-O stretching, and indicates that silica was successfully coated on MNPs (Fig. 3-c). The additional peaks appeared in the FTIR spectrum of magnetic GO-hydrogel nanocomposite (Fig. 3-d) are related to various functional groups present in the structure of hydrogel.

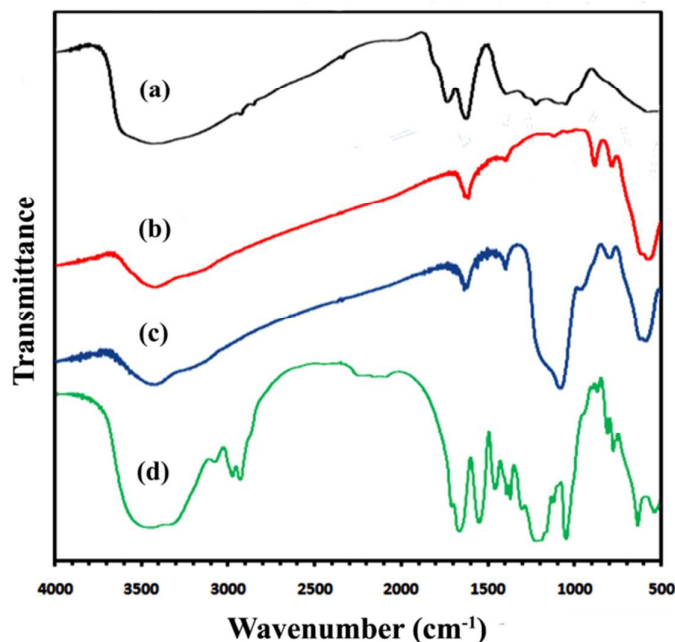


Fig. 3 FTIR spectra of GO (a), MNP (b), MNP@SiO₂ (c) and HGO1 (d)

TGA spectra of hydrogels with and without GO are illustrated in Fig. 4. The weight loss at about $100\text{ }^{\circ}\text{C}$ is attributed to the removal of adsorbed water molecules. Thermal degradation of both the samples occurs at two stages and about 70% weight loss was observed up to $600\text{ }^{\circ}\text{C}$. The onset of weight loss is at $280\text{ }^{\circ}\text{C}$ for HGO0 and at $320\text{ }^{\circ}\text{C}$ for HGO1 which indicates the presence of GO enhances thermal stability of hydrogels.

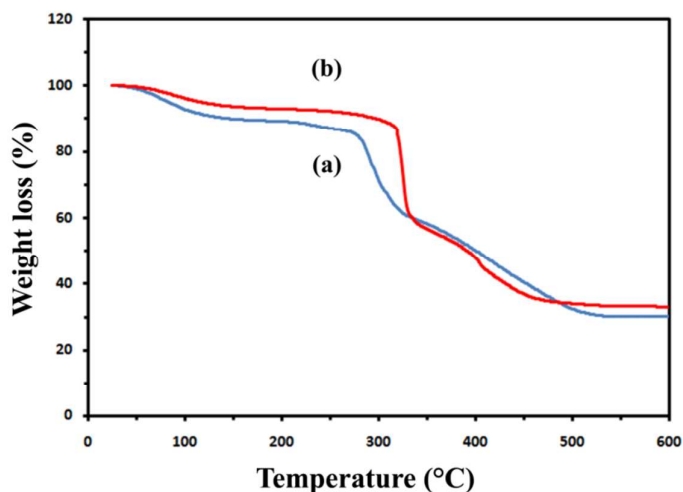


Fig. 4 TGA spectra of HGO0 (a) and HGO1 (b)

SEM and TEM images of hydrogel are shown in Fig. 5 and in Fig. S2 of ESI. SEM image shows that the synthesized hydrogels are porous and there are many pores with different sizes in their structure. The porosity of polymer is very important in adsorption process, because it increases surface area and enhances adsorption capacity. Porosity also affects on the rate of water diffusion. Water, and as a consequence the dyes dissolved in it, can easily diffuse through the porous structure of hydrogels and interact with functional groups present in the polymeric network. TEM image of hydrogel nanocomposite (Fig. 5-a) shows that magnetic nanoparticles with narrow size distribution are present in the structure of nanocomposite. These nanoparticles with sizes about 10 nm are well-dispersed in the polymeric matrix of hydrogel.

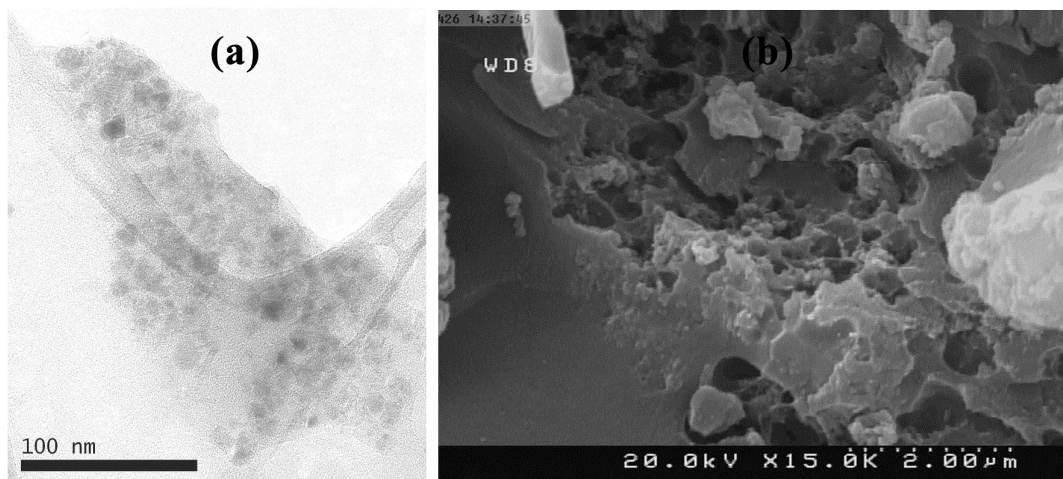


Fig. 5 TEM (a) and SEM (b) image of hydrogel nanocomposites

Magnetization curve of the prepared MNPs and nanocomposite hydrogels are shown in Fig. 6. Magnetic hysteresis loop of both samples exhibits superparamagnetic characteristic at room temperature. Saturation magnetization of MNP@SiO_2 is about 65 emu g^{-1} . Entrapment of MNP@SiO_2 into the hydrogel reduces saturation magnetization to about 22 emu g^{-1} . However it is still enough for magnetic separation of particles as can be seen from the inset of Fig. 6.

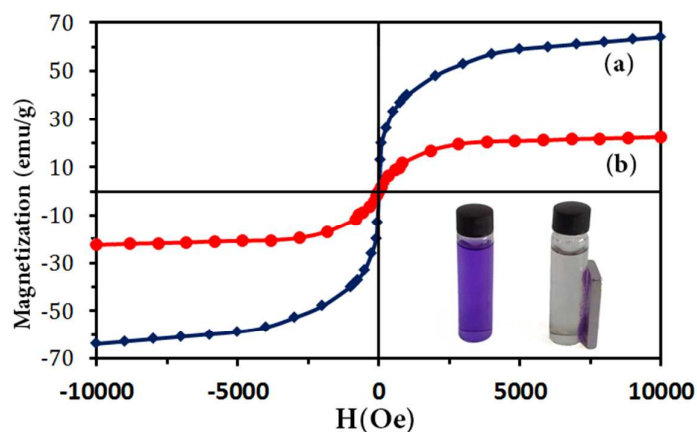


Fig. 6 Magnetization curve of MNPs (a) and hydrogel nanocomposite (b). (The inset shows magnetic separation of adsorbents from dye solution)

Dye adsorption

The synthesized hydrogels were used as dye adsorbents and their ability for dye adsorption was studied. The dye used here is CV which its structure is shown in Fig. S3 of ESI. Adsorption of CV from aqueous solution using hydrogels with different GO content was investigated. As shown in Fig. 7, the hydrogel without GO (HGO0) adsorbed CV to a maximum value of $q_e=67 \text{ mg g}^{-1}$. The hydrogel synthesized here contains many polar functional groups such as sulfonate and hydroxyl groups which are able to absorb dyes through electrostatic interactions and hydrogen bonds.

The results depicted in Fig. 7 shows that the presence of GO increases dye adsorption significantly. The adsorption capacity of dye is 77.07 mg g^{-1} for hydrogel containing 1 % GO (HGO1). The dye used in this experiment is CV which is a cationic dye. GO contains many functional groups which are able to interact with dye molecules. Negatively charged carboxylate groups on the surface of GO can interact with the cationic dye molecules through electrostatic attraction forces. Other polar oxygen-containing functional groups on the surface of GO interact with dyes too. For example hydroxyl groups can form hydrogen bonds with dye molecules. There are also aromatic non-functionalized regions in the structure of GO that affect on dye adsorption through π - π interactions. Another important property of GO is its high specific surface area which strongly affects on adsorption. Incorporation of GO into the hydrogels provides more surface area and facilitate dye adsorption. Although increasing GO content from 1% to 3% and 5% increased adsorption capacity, the differences were not significant. However, further increasing of GO content to 7 %, reduced adsorption capacity considerably. Based on the results obtained in this part, we chose HGO1 for further experiments.

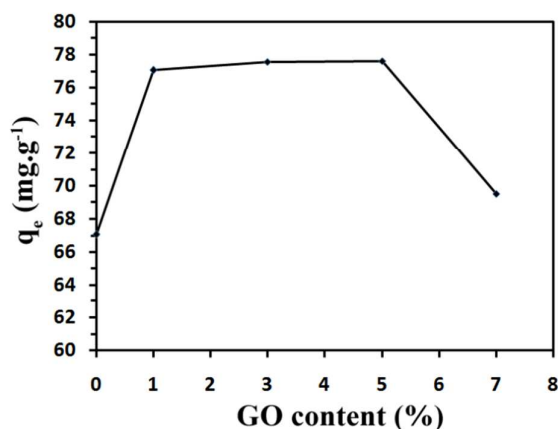


Fig. 7 The effect of GO content on adsorption capacity

Effect of pH

Adsorption measurements were performed in 50 mg L⁻¹ dye solutions with different pH adjusted by addition of HCl or NaOH solutions (0.01 N). As is shown in Fig. 8-a, adsorption capacity decreased with increasing pH. Electrostatic interaction is a very important parameter which can strongly affect on adsorption process. The adsorbent contains many sulfonate groups which, as a conjugated base of a strong acid, remain ionized at pH ranges of the experiment. In contrast, the molecules of CV contain tertiary amine groups and are cationic in acidic media, but are neutral and non-ionic in alkaline solutions. As a consequence, by increasing pH, the number of protonated cationic groups of dyes, and thus electrostatic interaction with adsorbent, decreases which reduces dye adsorption.

Effect of initial dye concentration

The effect of initial concentration of dye on adsorption capacity was evaluated and the results are shown in Fig. 8-b. Dye adsorption increased continuously from 77.07 to 712.09 mg g⁻¹ as the initial dye concentration increases in the range of 20 to 250 mg L⁻¹. It should be due to the fact that the driving force to overcome the mass transfer resistance of dye molecules from aqueous phase to solid phase is greater in higher dye concentrations.³¹ It should be noted that

the rate of increase in adsorption capacity decreases and finally reaches to a constant value by further increasing of initial dye concentration.

Effect of adsorbent dosage

Removal of CV from solution was also investigated using different amounts of adsorbent. Experiments were performed in a 50 mg L^{-1} dye solution. As shown in Fig. 8-c, an increase in adsorbent dosage leads to a significant decrease in adsorption capacity. By increasing adsorbent dosage from 10 to 90 mg, adsorption capacity continuously decreased from 180 to 20 mg g^{-1} . This observation is attributed to the splitting effect of flux or concentration gradient between dye molecules and adsorbent.³²

Effect of contact time

Fig. 8-d shows the effect of contact time on adsorption of CV on the adsorbents. It can be seen that adsorption capacity increases rapidly at the initial stages of adsorption. Adsorption is very fast in the first 15 minutes of the experiment and then increases slowly and reaches to equilibrium after 2 h. This is because vacant surface sites of the adsorbents are blocked within the first stages of the adsorption and thus diffusion and adsorption of further dye molecules becomes more difficult.

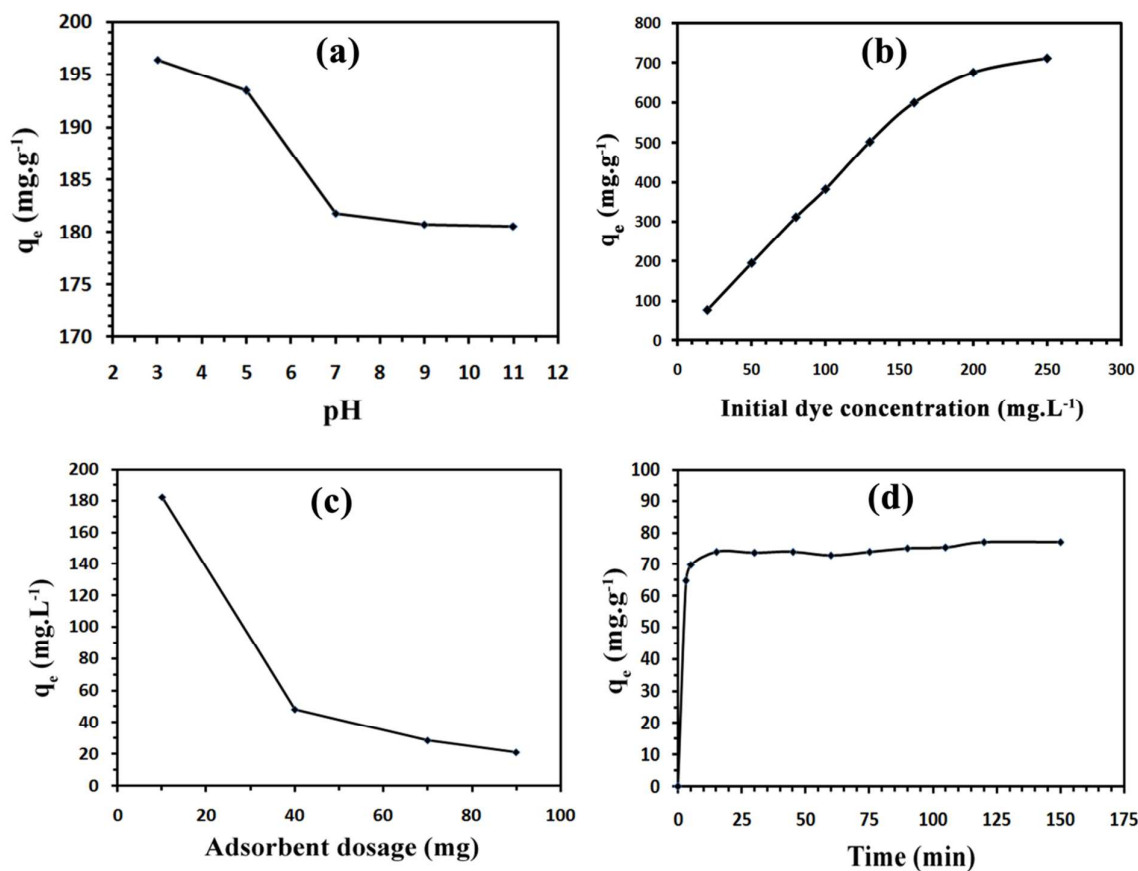


Fig. 8 The effect of pH (a), initial dye concentration (b), adsorbent dosage (c) and contact time (d) on adsorption capacity

Adsorption kinetic

Pseudo-first-order and pseudo-second-order models were employed to describe the kinetic of adsorption. Lagergren pseudo-first-order³³ and Ho pseudo-second-order³⁴ models are expressed as equations 3 and 4, respectively:

$$\log(q_e - q_t) = \log q_e - \left(\frac{k_1 t}{2.303} \right) \quad (3)$$

$$\frac{t}{q_t} = \frac{1}{k_2 q_e^2} + \frac{t}{q_e} \quad (4)$$

Where q_e and q_t are adsorption capacity (mg g^{-1}) at equilibrium and at time t (min) respectively, and k_1 and k_2 are pseudo-first-order constant (min^{-1}) and pseudo-second-order rate constant ($\text{g mg}^{-1} \text{min}^{-1}$), respectively.

The kinetic parameters for the two models were determined and listed in table 2. The results show that the correlation coefficient (R^2) for the pseudo-first-order model is very low, and there is a large difference between calculated adsorption capacity (q_{calc}) and experimental value (q_{exp}). The plots of pseudo-first-order and pseudo-second-order kinetic models are shown in Fig. S4 of ESI. As shown in this Figure, experimental data are better fitted with pseudo-second-order kinetic model. Coefficient factor for this model is very high ($R=0.999$) and calculated adsorption capacity is in good agreement with experimental value.

Table 2 Kinetic parameters for pseudo-first-order and pseudo-second-order models

kinetic model	parameters				
	K_1	K_2	q_e	R^2	q_{exp}
	min^{-1}	$\text{g mg}^{-1} \text{min}^{-1}$	mg g^{-1}		mg g^{-1}
pseudo-first-order	0.0507		20.94	0.482	77.07
pseudo-second-order		0.0094	76.92	0.999	77.07

Adsorption isotherm

The isotherm of CV adsorption on the nanocomposite hydrogels was studied by calculating adsorption capacity as a function of dye equilibrium concentration. The experimental data were analyzed by using Langmuir and Freundlich isotherm models. In Langmuir isotherm, the adsorbent surface is considered homogeneous with identical and energetically equivalent sorption sites. Langmuir model is expressed as follows:³⁵

$$\frac{1}{q_e} = \frac{1}{C_e K_L q_m} + \frac{1}{q_m} \quad (5)$$

Where C_e is dye equilibrium concentration (mg g^{-1}), K_L is Langmuir adsorption constant related to the energy of adsorption (L mg^{-1}), q_m is maximum adsorption capacity (mg g^{-1}).

Freundlich isotherm model is based on adsorption on heterogeneous adsorption surface and is expressed as follows:³⁶

$$\log q_e = \log K_F + \frac{1}{n} \log C_e \quad (6)$$

Where C_e is dye equilibrium concentration (mg L^{-1}), K_F is Freundlich constant (L g^{-1}) and n is heterogeneity factor.

The related parameters for the two models were calculated and are represented in table 3. Higher coefficient factor of Langmuir isotherm ($R^2=0.974$), implies that this model provides a better fit of the experimental data and properly describes adsorption equilibrium of CV on the prepared adsorbents. The curve related to Langmuir and Freundlich isotherm equations are shown in Fig. S5 of ESI.

Table 3 Isotherm parameters for Langmuir and Freundlich models

isotherm model	parameters				
	K_F $\text{mg g}^{-1} (\text{L mg}^{-1})^{1/n}$	K_L L mg^{-1}	q_m mg g^{-1}	n	R^2
Langmuir		0.325	769.23		0.974
Freundlich	7.6			3.45	0.818

A dimensionless constant called the equilibrium parameter (R_L) is used to predict whether an adsorption system is favorable or unfavorable. This constant is defined as:³⁷

$$R_L = \frac{1}{1+K_L C_0} \quad (7)$$

Where K_L and C_0 are Langmuir adsorption constant and initial dye concentration, respectively. The value of R_L indicates the adsorption process to be either unfavorable ($R_L > 1$), linear ($R_L = 1$), favorable ($0 < R_L < 1$), or irreversible ($R_L = 0$). The values of R_L at different initial CV concentrations are shown in Fig. S6 of ESI. It is clear that the R_L values are between 0 and 1 indicating adsorption of CV on prepared adsorbents is favorable.

Recycling study

In order to study reusability of the adsorbents, the particles were separated after adsorption process by using a magnet. The dyes were desorbed by 2 h stirring in 20 mL acetone and the adsorbents were dried at 40 °C. The recycled adsorbents were used for next adsorption runs. The results of recycling experiment for 5 cycles are shown in Fig. 15. It is observed that about 96 % of the dyes were removed after the first cycle. As is shown in Fig. 9, the removal efficiency did not change significantly even after five cycles of adsorption-desorption. The presence of magnetic nanoparticles facilitates separation and recycling of adsorbents, as shown in the inset of Fig. 6.

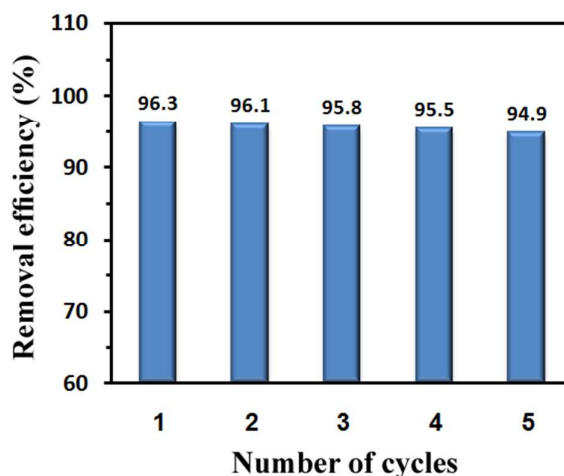


Fig. 9 Reusability of the adsorbents

Comparison with other adsorbents

For a better understanding of the adsorption ability of the prepared particles, we compared the results obtained here with some other adsorbents that have been used for CV removal.

Langmuir maximum adsorption capacity and conditions used for adsorption experiment are listed in table 4. It can be seen that the adsorbent used in this study shows much higher adsorption capacity than the other adsorbents. Considering other parameters such as contact time and pH of the solution reveals that the adsorbent prepared here can be considered as a suitable and highly efficient adsorbent for CV.

For being used in large scale water purification, an adsorbent should have low cost, high adsorption capacity, high mechanical strength and reusability. Hydrogels can be considered as a good candidate for dye adsorption since they can be prepared from low cost materials such as natural polysaccharides. The presence of fillers which increase the mechanical strength of the hydrogels and facilitate their reusability can enhance the potential using of hydrogels practically.

Table 4 Comparison with other adsorbents

adsorbent	contact time	q _m	pH	reference
	min	mg g ⁻¹		
Semi-IPN Poly(AA-AAm-MA)/amylose ^a	3000	35.09	7.4	38
Sulfated MCM-41	150	138.7	7	39
Palm kernel fiber	60	78.9	7.2	40
Kaoline	5	47.27	7	41
PAA Bound Magnetic Nanoparticles	1	116	6	42
CGS ^b	150	182.15	9	43
Cu(II)-Loaded Montmorillonite	300	114.3	8.2	44
Magnetic GO/hydrogel nanocomposite	120	769.23	7	This study

^a semi-IPN hydrogels constituted of poly(acrylic acid-acrylamide-methacrylate) and amylose

^b cellulose modified with glycidyl methacrylate and sulfosalicylic acid

Conclusions

In summary, we have synthesized GO-containing polymeric nanocomposites which are composed of crosslinked PAMPS and starch. The prepared hydrogels were used as adsorbents for removal of CV and a very high adsorption capacity (769.23 mg g^{-1}) was obtained. The results also revealed that the presence of GO has a significant effect on adsorption capacity. The effect of other experimental conditions such as pH of the solution, contact time, adsorbent dosage and initial dye concentration on adsorption capacity were also investigated. Adsorption capacity increased with increasing contact time and initial dye concentration and decreasing pH and adsorbent dosage. Study of the kinetic and isotherm of adsorption indicated that dye adsorption is well-described by pseudo-second-order and Langmuir models, respectively. The adsorbents were regenerated and reused for several cycles of adsorption-desorption and no significant reduction in removal efficiency was observed even after 5 cycles.

References

- 1 K. Singh and S. Arora, *Crit. Rev. Env. Sci. Technol.*, 2011, **41**, 807-878.
- 2 A. Anastasi, V. Prigione and G. C. Varese, *J. Hazard. Mater.*, 2010, **177**, 260-267.
- 3 Q. Zhang, T. Zhang, T. He, L. Chen, *Appl. Clay Sci.*, 2014, **90**, 1-5.
- 4 M. Arulkumar, P. Sathishkumar and T. Palvannan, *J. Hazard. Mater.*, 2011, **186**, 827-834.
- 5 C. Tian, Q. Zhang, A. Wu, M. Jiang, Z. Liang, B. Jiang, and H. Fu, *Chem. Commun.*, 2012, **48**, 2858-2860.
- 6 A. K. Verma, R. R. Dash and P. Bhunia, *J. Environ. Manage.*, 2012, **93**, 154-168.
- 7 M. Greluk and Z. Hubicki, *Chem. Eng. J.*, 2010, **162**, 919-926.
- 8 S. Cheng, D. L. Oatley, P. M. Williams and C. J. Wright, *Water Res.*, 2012, **46**, 33-42.
- 9 G. Mezohegyi, F. P. van der Zee, J. Font, A. Fortuny and A. Fabregat, *J. Environ. Manage.*, 2012, **102**, 148-164.
- 10 A. S. Bhatt, P. L. Sakaria, M. Vasudevan, R. R. Pawar, N. Sudheesh, H. C. Bajaj and H. M. Mody, *RSC Adv.*, 2012, **2**, 8663-8671.
- 11 A. K. Mishra, T. Arockiadoss and S. Ramaprabhu, *Chem. Eng. J.*, 2010, **162**, 1026-1034.
- 12 N. B. Shukla, S. Rattan and G. Madras, *Ind. Eng. Chem. Res.*, 2012, **51**, 14941-14948.
- 13 E. Yavuz, G. Bayramoğlu, M. Y. Arica and B. F. Senkal, *J. Chem. Technol. Biotechnol.*, 2011, **86**, 699-705.
- 14 V. V. Panic, Z. P. Madzarevic, T. Volkov-Husovic and S. J. Velickovic, *Chem. Eng. J.*, 2013, **217**, 192-204.
- 15 S. Li, H. Zhang, J. Feng, R. Xu and X. Liu, *Desalination*, 2011, **280**, 95-102.
- 16 S. Li, X. Liu, W. Huang, W. Li, X. Xia, S. Yan and J. Yu, *Polym. Adv. Technol.*, 2011, **22**, 2439-2447.
- 17 C. W. Chang, A. Spreeuwel, C. Zhanga and S. Varghese, *Soft Matter*, 2010, **6**, 5157-5164.

- 18 S. Chatterjee, M. W. Lee, and S. H. Woo, *Bioresour. Technol.*, 2010, **101**, 1800-1806.
- 19 L. Zhang, Z. Wang, C. Xu, Y. Li, J. Gao, W. Wangc and Y. Liu, *J. Mater. Chem.*, 2011, **21**, 10399-10406.
- 20 A. Ü. Metin, H. Çiftçi and E. Alver, *Ind. Eng. Chem. Res.*, 2013, **52**, 10569–10581
- 21 Y. Zhu, S. Murali, W. Cai, X. Li, J. W. Suk, J. R. Potts and R. S. Ruoff, *Adv. Mater.*, 2010, **22**, 3906-3924.
- 22 D. Chen, H. Feng and J. Li, *Chem. Rev.*, 2012, **112**, 6027-6053.
- 23 J. Fan, Z. Shi, M. Lian, H. Li and J. Yin, *J. Mater. Chem. A*, 2013, **1**, 7433-7443.
- 24 F. Liu, S. Chung, G. Oh and T. S. Seo, *ACS Appl. Mater. Interfaces*, 2012, **4**, 922-927.
- 25 Y. Zhou, S. Fu, H. Liu, S. Yang and H. Zhan, *Polym. Eng. Sci.*, 2011, **51**, 2417-2424.
- 26 A. Pourjavadi, S. H. Hosseini, F. Seidi and R. Soleyman, *Polym. Int.*, 2013, **62**, 1038-1044.
- 27 O. V. Kharissova, H. V. R. Dias, and B. I. Kharisov, *RSC Adv.*, 2015, **5**, 6695-6719.
- 28 Y. F. Lin and C. V. Chang, *RSC Adv.*, 2014, **4**, 28628-28631.
- 29 D. C. Marcano, D. V. Kosynkin, J. M. Berlin, A. Sinitskii, Z. Sun, A. Slesarev, L. B. Alemany, W. Lu and J. M. Tour, *ACS Nano*, 2010, **4**, 4806-4814.
- 30 C. Elvira, J.F. Mano, J. San Román, R. L. Reis, *Biomaterials*, 2002, **23**, 1955-1966.
- 31 Y. Zhou, M. Zhang, X. Hu, X. Wang, J. Niu and T. Ma, *J. Chem. Eng. Data*, 2013, **58**, 413-421.
- 32 A. Metin, H. Çiftçi and E. Alver, *Ind. Eng. Chem. Res.*, 2013, **52**, 10569-10581.
- 33 S. Lagergren, *K. Sven. Vetenskapsakad. Handl.*, 1898, **24**, 1-39.
- 34 Y. S. Ho, G. McKay, *Chem. Eng. J.*, 1998, **70**, 115-124.
- 35 I. Langmuir, *J. Am. Chem. Soc.*, 1916, **38**, 2221-2295.
- 36 H. M. F. Freundlich, *Z. Phys. Chem.*, 1906, **57**, 385–471.
- 37 T. W. Weber and R. K. Chakravorti, *AIChE J.* 1974, **20**, 228-238.

- 38 S. Li, *Bioresour. Technol.*, 2010, **101**, 2197-2202.
- 39 P. Monash and G. Pugazhenti, *Adsorption*, 2009, **15**, 390-405.
- 40 G. O. El-Sayed, *Desalination*, 2011, **272**, 225-232.
- 41 B. Nandi, A. Goswami, A. Das, B. Mondal, M. Purkait, *Sep. Sci. Technol.*, 2008, **43**, 1382-1403.
- 42 M. H. Liao, K. Y. Wu and D. H. Chen, *Sep. Sci. Technol.*, 2005, **39**, 1563-1575.
- 43 Y. Zhou, M. Zhang, X. Wang, Q. Huang, Y. Min, T. Ma and J. Niu, *Ind. Eng. Chem. Res.*, 2014, **53**, 5498-5506.
- 44 X. S. Wang and W. Zhang, *Sep. Sci. Technol.*, 2011, **46**, 656-663.